Oral presentation | Numerical methods

Numerical methods-VIII

Fri. Jul 19, 2024 10:45 AM - 12:45 PM Room A

[13-A-02] A hybrid nodal solver with rotation property for the cell-centered Lagrangian scheme

*Chunyuan Xu[1], Zhijun Shen[1], Qinghong Zeng[1] （1. Institute of Applied Physics and Computational Mathematics）

Keywords: Lagrangian methods, Rankine–Hugoniot condition, hybrid nodal solver

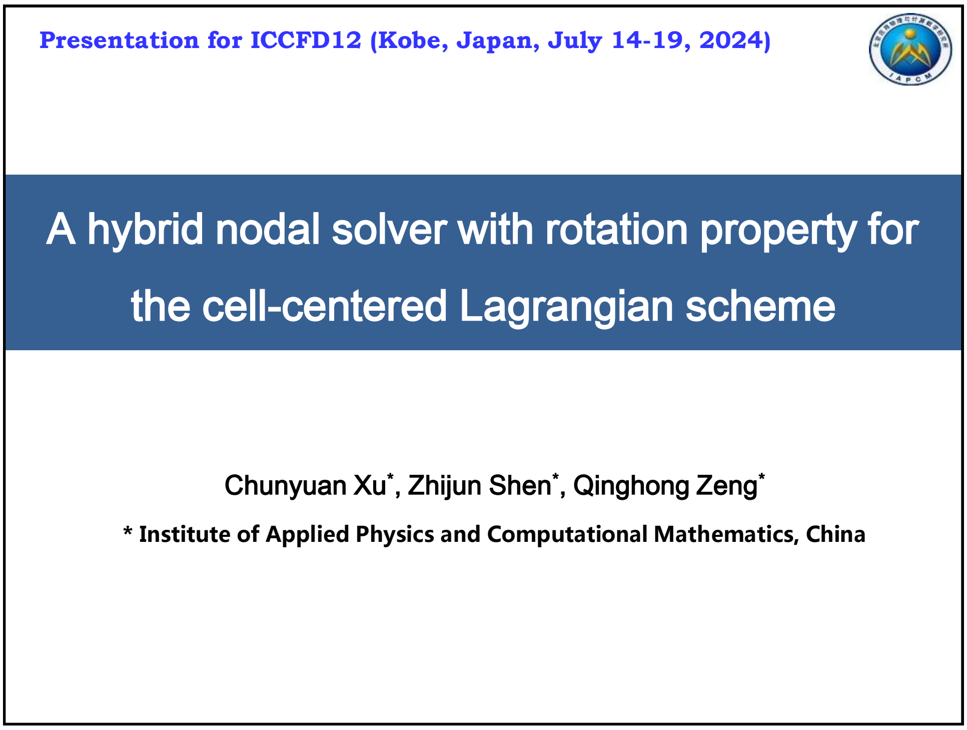

Presentation for ICCFD12 (Kobe, Japan, July 14-19, 2024)

A hybrid nodal solver with rotation property for the cell-centered Lagrangian scheme

Chunyuan Xu*, Zhijun Shen*, Qinghong Zeng*

* Institute of Applied Physics and Computational Mathematics, China

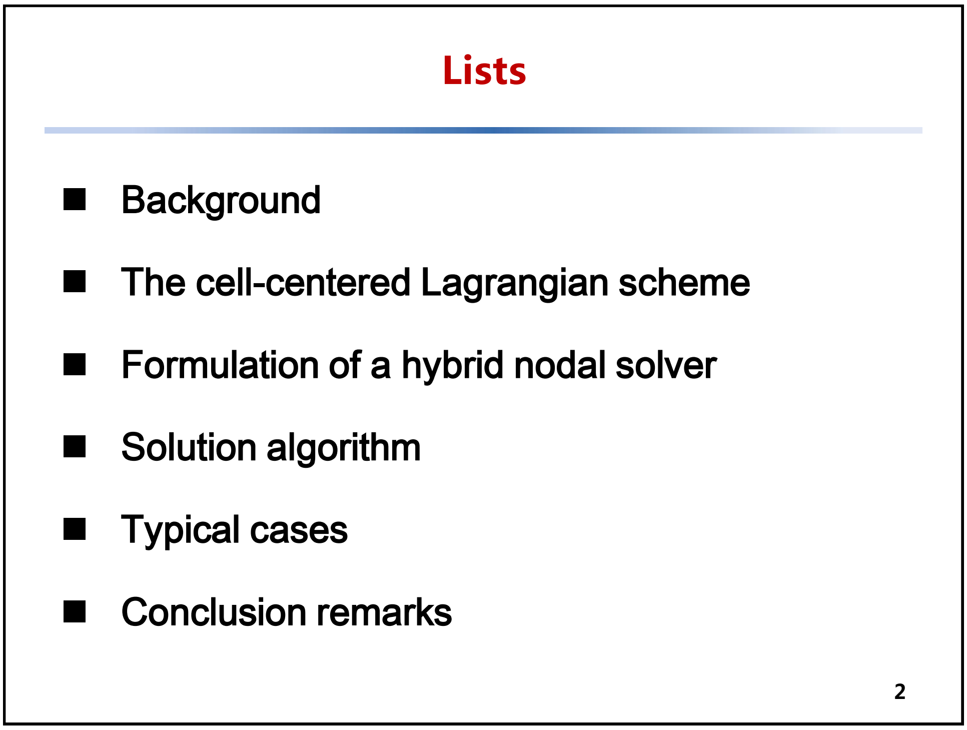

Lists

- Background
- The cell-centered Lagrangian scheme
- Formulation of a hybrid nodal solver
- Solution algorithm
- Typical cases
- Conclusion remarks

2

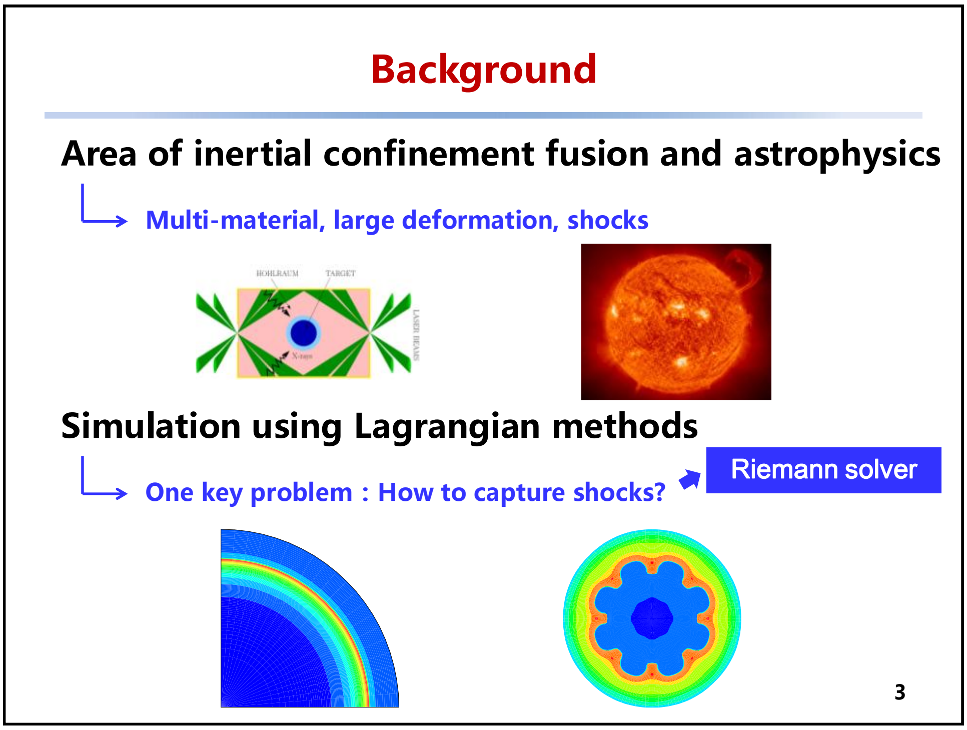

Background

Area of inertial confinement fusion and astrophysics

Multi-material, large deformation, shocks

HOHLRAUM
TARGET
LASER BEAMS
X-rays

Simulation using Lagrangian methods

One key problem：How to capture shocks?

Riemann solver

3

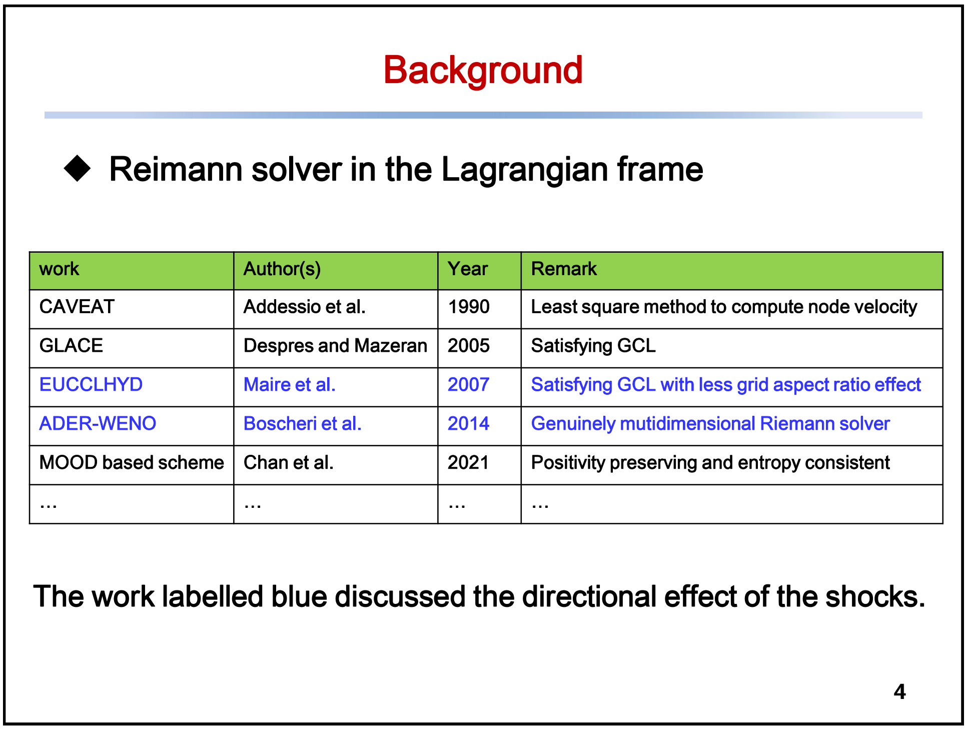

Background

- Reimann solver in the Lagrangian frame

work	Author(s)	Year	Remark
CAVEAT	Addessio et al.	1990	Least square method to compute node velocity
GLACE	Despres and Mazeran	2005	Satisfying GCL
EUCCLHYD	Maire et al.	2007	Satisfying GCL with less grid aspect ratio effect
ADER-WENO	Boscheri et al.	2014	Genuinely mutidimensional Riemann solver
MOOD based scheme	Chan et al.	2021	Positivity preserving and entropy consistent
…	…	…	…

The work labelled blue discussed the directional effect of the shocks.

4

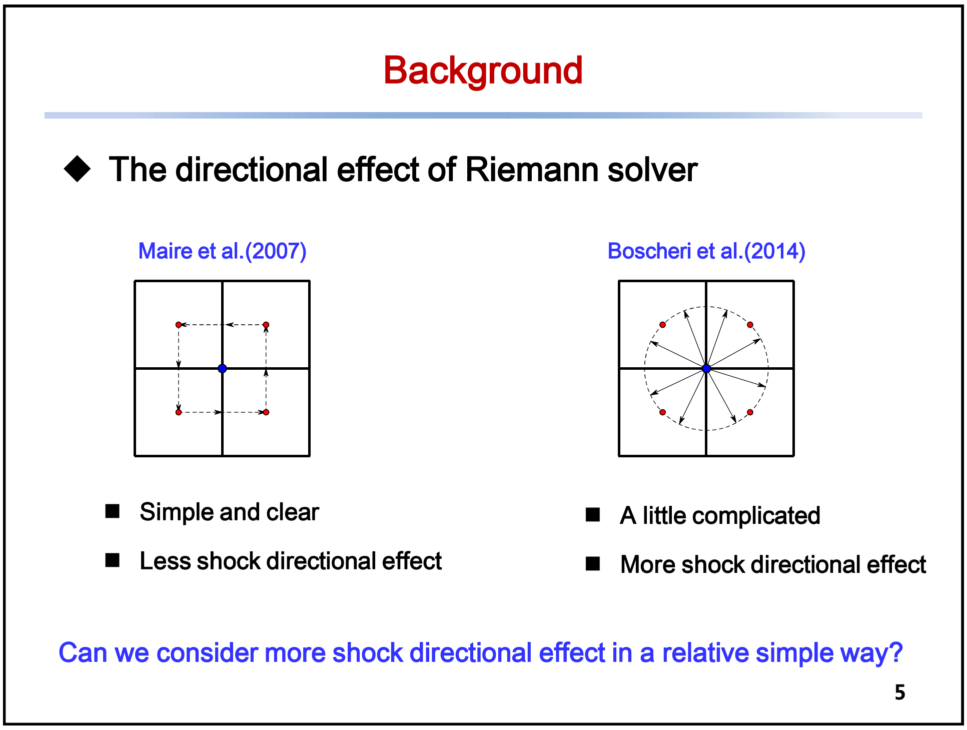

Background

- The directional effect of Riemann solver

- Simple and clear
- Less shock directional effect

- A little complicated
- More shock directional effect

Can we consider more shock directional effect in a relative simple way?

5

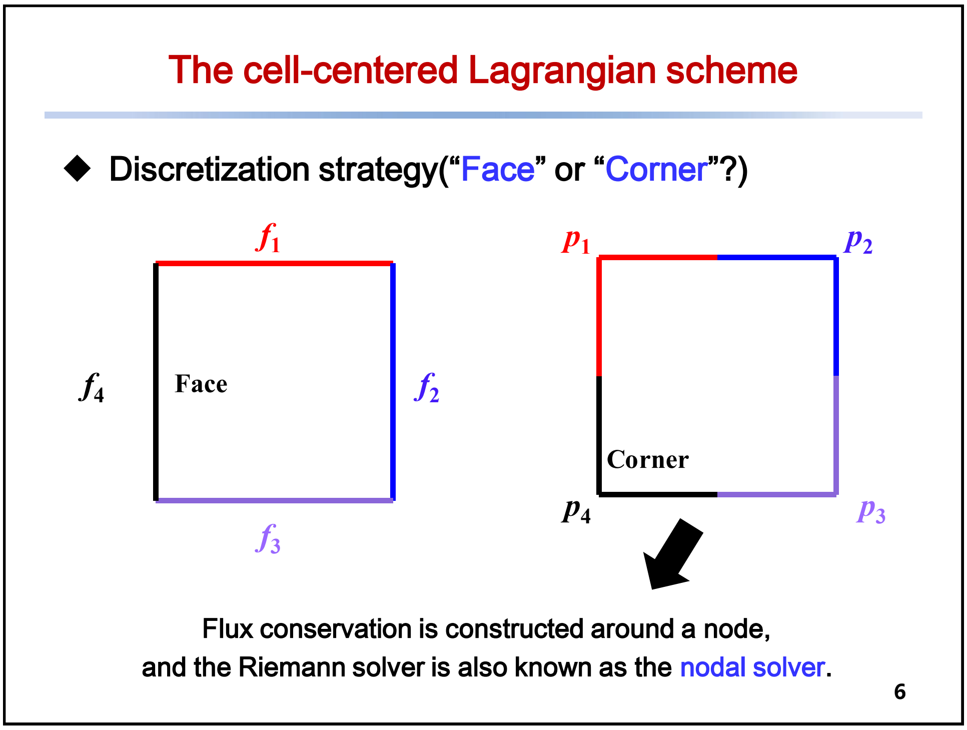

The cell-centered Lagrangian scheme

- Discretization strategy("Face" or "Corner"?)

Flux conservation is constructed around a node,
and the Riemann solver is also known as the nodal solver.

6

The cell-centered Lagrangian scheme

- Finite volume scheme (Maire, 2009)

$$m_c\frac{d}{dt}(\frac{1}{\rho_c}) - \sum_{p\in\mathcal{P}(c)} \left(L_{\underline{p}}^c \boldsymbol{N}_{\underline{p}}^c + L_{\overline{p}}^c \boldsymbol{N}_{\overline{p}}^c\right) \cdot \boldsymbol{U}_p = 0,$$

$$m_c\frac{d}{dt}\boldsymbol{U}_c + \sum_{p\in\mathcal{P}(c)} \left(L_{\underline{p}}^c \Pi_{\underline{p}}^c \boldsymbol{N}_{\underline{p}}^c + L_{\overline{p}}^c \Pi_{\overline{p}}^c \boldsymbol{N}_{\overline{p}}^c\right) = \boldsymbol{0},$$

$$m_c\frac{d}{dt}E_c + \sum_{p\in\mathcal{P}(c)} \left(L_{\underline{p}}^c \Pi_{\underline{p}}^c \boldsymbol{N}_{\underline{p}}^c + L_{\overline{p}}^c \Pi_{\overline{p}}^c \boldsymbol{N}_{\overline{p}}^c\right) \cdot \boldsymbol{U}_p = 0.$$

□ Least square method and two-step Runge-Kutta method.

[1] Maire, A high-order cell-centered Lagrangian scheme for two-dimensional compressible fluid flows on unstructured meshes, JCP, 2008.

Formulation of a hybrid nodal solver

- Lagrangian Rankine-Hugoniot condition

$$-s\Delta \boldsymbol{U} + \Delta \boldsymbol{F} = 0$$

where $\boldsymbol{U} = (V, u, E)^t$ and $\boldsymbol{F} = (-u, P, Pu)^t$.

In multi-dimensions, the momentum RH condition writes

$$\Delta \boldsymbol{f} = s\Delta \boldsymbol{u}$$

□ $\Delta \boldsymbol{u}$ is regarded as a component of a vector;

□ $\Delta \boldsymbol{u}$ is regarded as the projection of the velocity gradient along a certain direction.

We will always use this assumption!

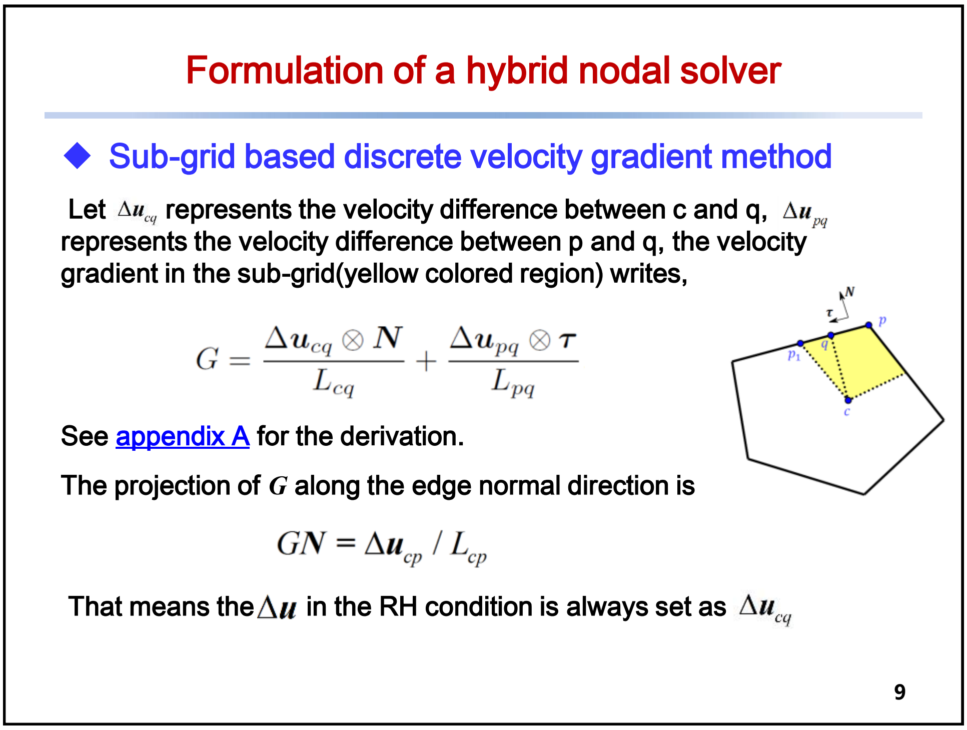

Formulation of a hybrid nodal solver

◆ Sub-grid based discrete velocity gradient method

Let $\Delta \boldsymbol{u}_{cq}$ represents the velocity difference between c and q, $\Delta \boldsymbol{u}_{pq}$ represents the velocity difference between p and q, the velocity gradient in the sub-grid(yellow colored region) writes,

$$G = \frac{\Delta \boldsymbol{u}_{cq} \otimes \boldsymbol{N}}{L_{cq}} + \frac{\Delta \boldsymbol{u}_{pq} \otimes \boldsymbol{\tau}}{L_{pq}}$$

See appendix A for the derivation.

The projection of G along the edge normal direction is

$$G\boldsymbol{N} = \Delta \boldsymbol{u}_{cp} \,/\, L_{cp}$$

That means the $\Delta \boldsymbol{u}$ in the RH condition is always set as $\Delta \boldsymbol{u}_{cq}$

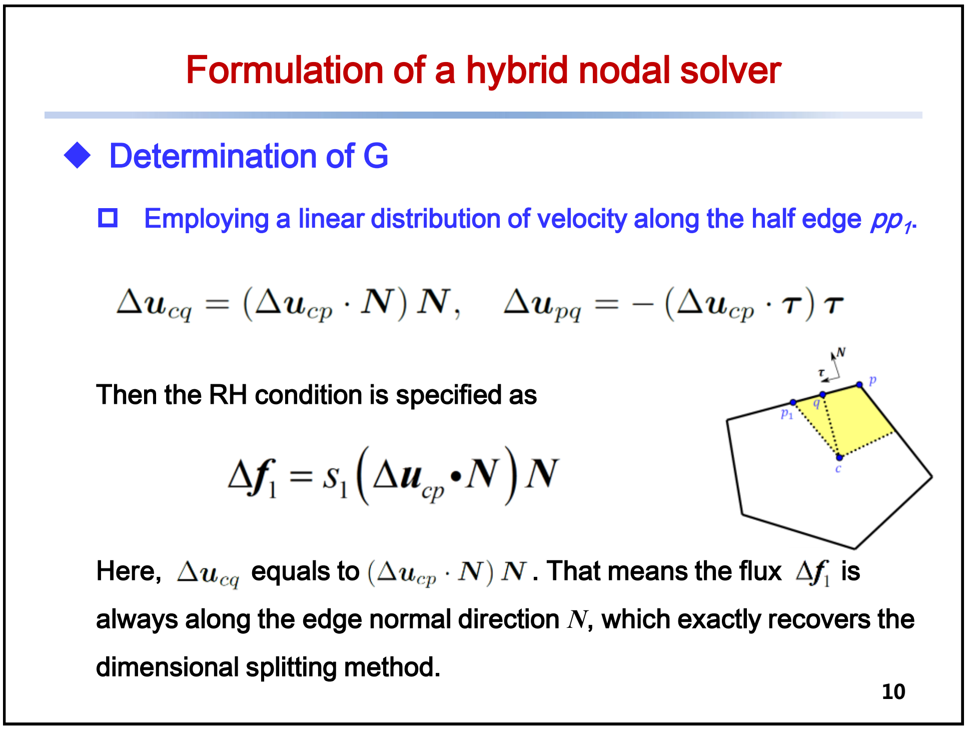

Formulation of a hybrid nodal solver

◆ Determination of G

- □ Employing a linear distribution of velocity along the half edge *pp₁*.

$$\Delta \boldsymbol{u}_{cq} = (\Delta \boldsymbol{u}_{cp} \cdot \boldsymbol{N})\,\boldsymbol{N}, \quad \Delta \boldsymbol{u}_{pq} = -(\Delta \boldsymbol{u}_{cp} \cdot \boldsymbol{\tau})\,\boldsymbol{\tau}$$

Then the RH condition is specified as

$$\Delta \boldsymbol{f}_1 = s_1 \left(\Delta \boldsymbol{u}_{cp} \bullet \boldsymbol{N} \right) \boldsymbol{N}$$

Here, $\Delta \boldsymbol{u}_{cq}$ equals to $(\Delta \boldsymbol{u}_{cp} \cdot \boldsymbol{N})\,\boldsymbol{N}$. That means the flux $\Delta \boldsymbol{f}_1$ is always along the edge normal direction $\boldsymbol{N}$, which exactly recovers the dimensional splitting method.

Formulation of a hybrid nodal solver

◆ Determination of G

□ Employing a constant distribution of velocity along *pp₁*.

$$\Delta \boldsymbol{u}_{cq} = \Delta \boldsymbol{u}_{cp}, \quad \Delta \boldsymbol{u}_{pq} = 0$$

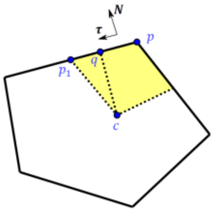

Then the RH condition is specified as

$$\Delta \boldsymbol{f}_2 = s_2 \Delta \boldsymbol{u}_{cp}$$

Here, $\Delta \boldsymbol{u}_{cq}$ equals to $\Delta \boldsymbol{u}_{cp}$. That means the flux $\Delta \boldsymbol{f}_2$ is always along the direction *of* $\Delta \boldsymbol{u}_{cp}$.

11

Formulation of a hybrid nodal solver

◆ Determination of the coefficient s

The amount of dissipation introduced by the two assumptions should be identical since they both solve a standard discontinuity problem,

$$\Delta \boldsymbol{f}_1 = \Delta \boldsymbol{f}_2 \quad \Rightarrow \quad s_2 = s_1 \frac{\left|\Delta \boldsymbol{u}_{cp} \bullet \boldsymbol{N}\right|}{\left|\Delta \boldsymbol{u}_{cp}\right|}$$

□ The two different fluxes are introduced by assuming different velocity distribution along the half edge;

□ $\Delta \boldsymbol{f}_2$ could be regarded as a rotation of $\Delta \boldsymbol{f}_1$ from the $\boldsymbol{N}$ direction to the $\Delta \boldsymbol{u}_{cp}$ direction.

12

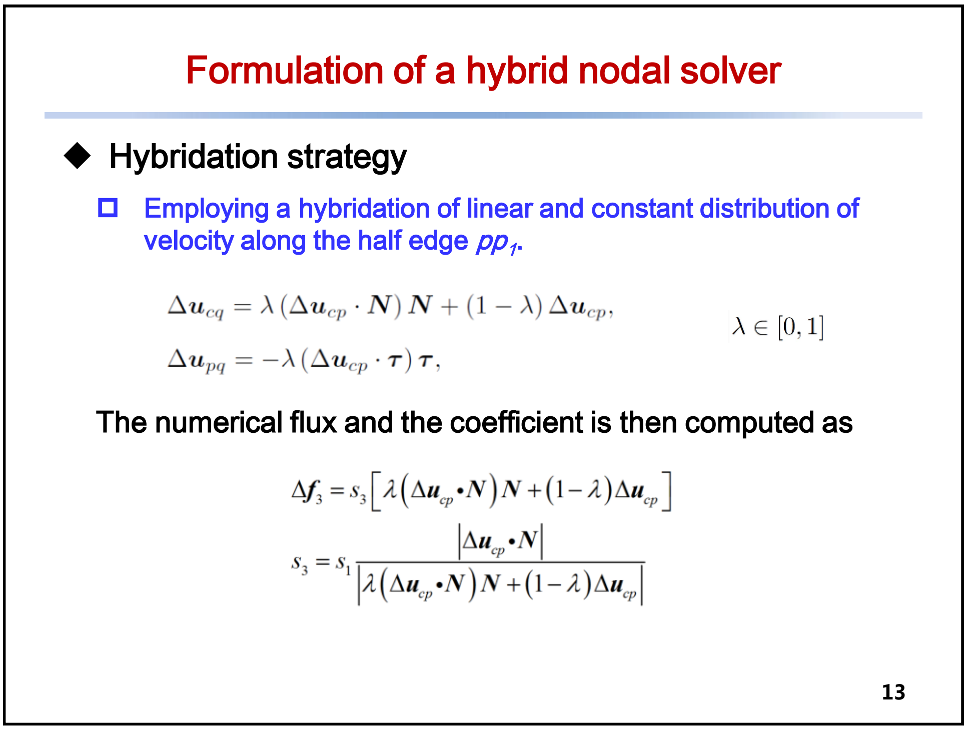

Formulation of a hybrid nodal solver

- Hybridation strategy
  - □ Employing a hybridation of linear and constant distribution of velocity along the half edge *pp₁*.

$$\Delta \boldsymbol{u}_{cq} = \lambda \left(\Delta \boldsymbol{u}_{cp} \cdot \boldsymbol{N}\right) \boldsymbol{N} + (1-\lambda)\, \Delta \boldsymbol{u}_{cp}, \qquad \lambda \in [0,1]$$

$$\Delta \boldsymbol{u}_{pq} = -\lambda \left(\Delta \boldsymbol{u}_{cp} \cdot \boldsymbol{\tau}\right) \boldsymbol{\tau},$$

The numerical flux and the coefficient is then computed as

$$\Delta \boldsymbol{f}_3 = s_3 \left[\lambda \left(\Delta \boldsymbol{u}_{cp} \bullet \boldsymbol{N}\right) \boldsymbol{N} + (1-\lambda) \Delta \boldsymbol{u}_{cp}\right]$$

$$s_3 = s_1 \frac{\left|\Delta \boldsymbol{u}_{cp} \bullet \boldsymbol{N}\right|}{\left|\lambda \left(\Delta \boldsymbol{u}_{cp} \bullet \boldsymbol{N}\right) \boldsymbol{N} + (1-\lambda) \Delta \boldsymbol{u}_{cp}\right|}$$

13

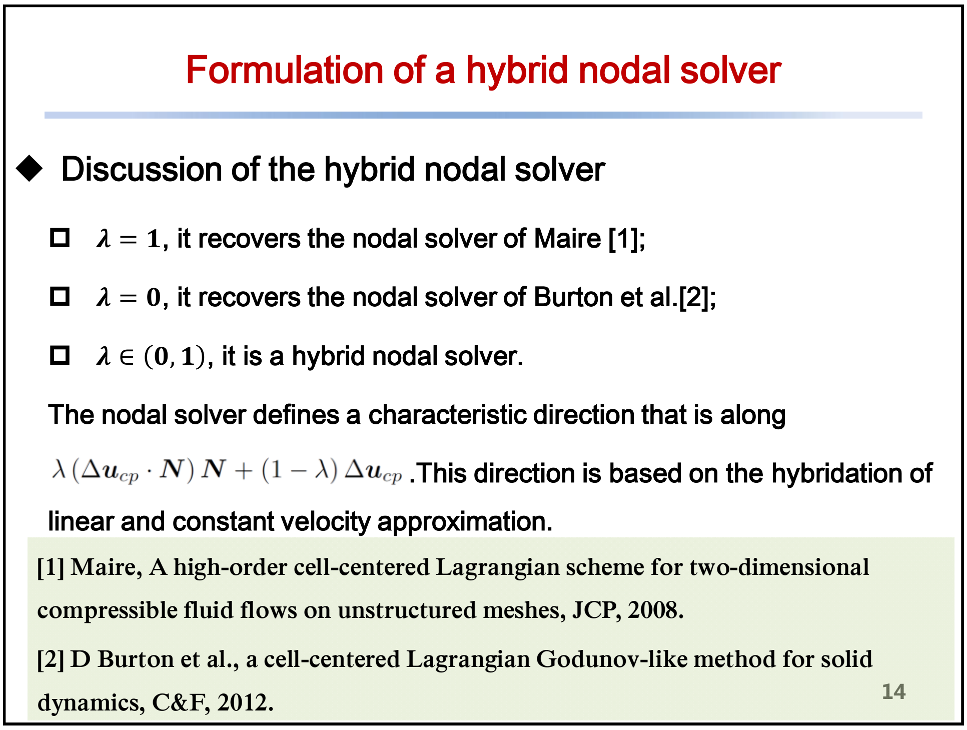

Formulation of a hybrid nodal solver

- Discussion of the hybrid nodal solver
  - □ $\lambda = 1$, it recovers the nodal solver of Maire [1];
  - □ $\lambda = 0$, it recovers the nodal solver of Burton et al.[2];
  - □ $\lambda \in (0, 1)$, it is a hybrid nodal solver.

The nodal solver defines a characteristic direction that is along $\lambda \left(\Delta \boldsymbol{u}_{cp} \cdot \boldsymbol{N}\right) \boldsymbol{N} + (1-\lambda)\, \Delta \boldsymbol{u}_{cp}$ .This direction is based on the hybridation of linear and constant velocity approximation.

[1] Maire, A high-order cell-centered Lagrangian scheme for two-dimensional compressible fluid flows on unstructured meshes, JCP, 2008.

[2] D Burton et al., a cell-centered Lagrangian Godunov-like method for solid dynamics, C&F, 2012.

14

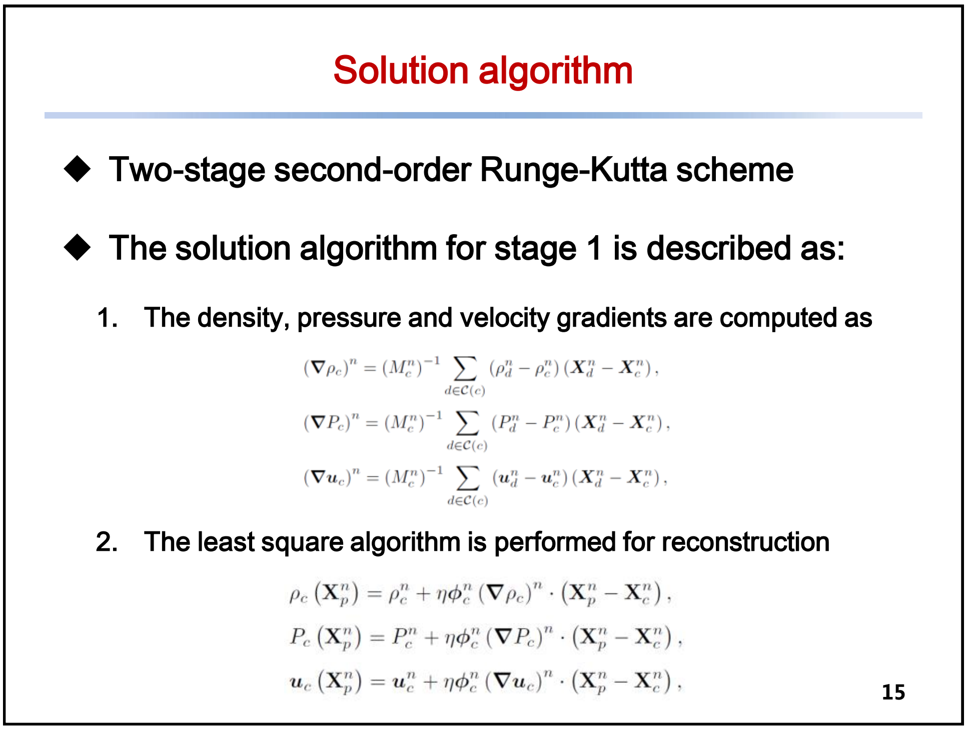

Solution algorithm

- Two-stage second-order Runge-Kutta scheme
- The solution algorithm for stage 1 is described as:

1. The density, pressure and velocity gradients are computed as

$$(\boldsymbol{\nabla}\rho_c)^n = (M_c^n)^{-1} \sum_{d\in\mathcal{C}(c)} (\rho_d^n - \rho_c^n)(\boldsymbol{X}_d^n - \boldsymbol{X}_c^n),$$

$$(\boldsymbol{\nabla}P_c)^n = (M_c^n)^{-1} \sum_{d\in\mathcal{C}(c)} (P_d^n - P_c^n)(\boldsymbol{X}_d^n - \boldsymbol{X}_c^n),$$

$$(\boldsymbol{\nabla}\boldsymbol{u}_c)^n = (M_c^n)^{-1} \sum_{d\in\mathcal{C}(c)} (\boldsymbol{u}_d^n - \boldsymbol{u}_c^n)(\boldsymbol{X}_d^n - \boldsymbol{X}_c^n),$$

2. The least square algorithm is performed for reconstruction

$$\rho_c\left(\mathbf{X}_p^n\right) = \rho_c^n + \eta\phi_c^n\left(\boldsymbol{\nabla}\rho_c\right)^n \cdot \left(\mathbf{X}_p^n - \mathbf{X}_c^n\right),$$

$$P_c\left(\mathbf{X}_p^n\right) = P_c^n + \eta\phi_c^n\left(\boldsymbol{\nabla}P_c\right)^n \cdot \left(\mathbf{X}_p^n - \mathbf{X}_c^n\right),$$

$$\boldsymbol{u}_c\left(\mathbf{X}_p^n\right) = \boldsymbol{u}_c^n + \eta\phi_c^n\left(\boldsymbol{\nabla}\boldsymbol{u}_c\right)^n \cdot \left(\mathbf{X}_p^n - \mathbf{X}_c^n\right),$$

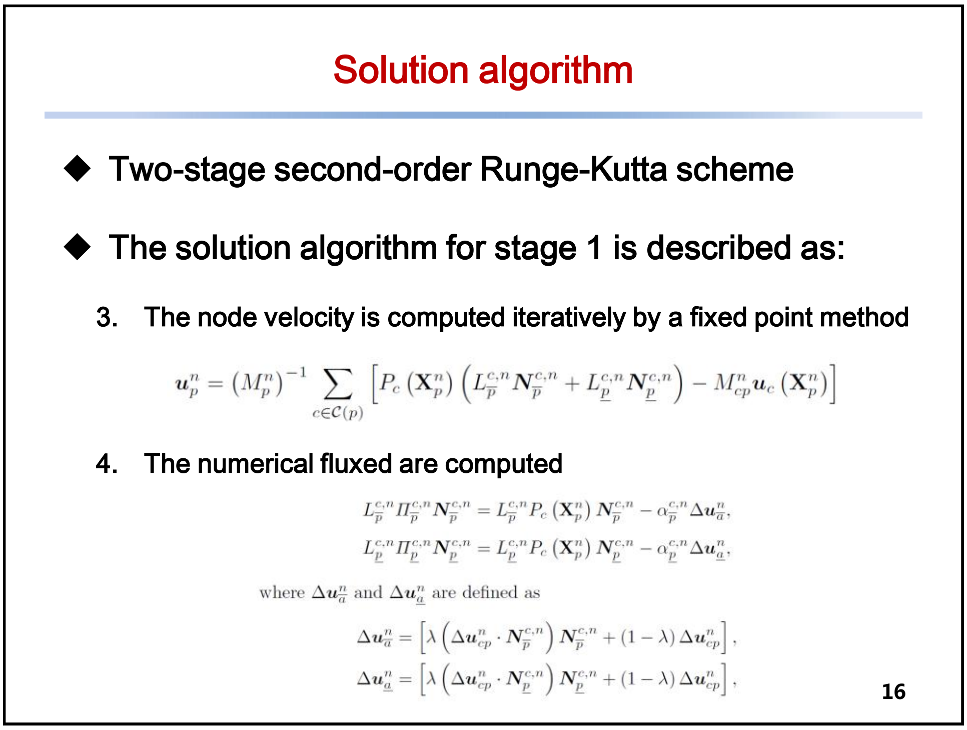

Solution algorithm

- Two-stage second-order Runge-Kutta scheme
- The solution algorithm for stage 1 is described as:

3. The node velocity is computed iteratively by a fixed point method

$$\boldsymbol{u}_p^n = (M_p^n)^{-1} \sum_{c\in\mathcal{C}(p)} \left[P_c\left(\mathbf{X}_p^n\right)\left(L_{\overline{p}}^{c,n}\boldsymbol{N}_{\overline{p}}^{c,n} + L_{\underline{p}}^{c,n}\boldsymbol{N}_{\underline{p}}^{c,n}\right) - M_{cp}^n\boldsymbol{u}_c\left(\mathbf{X}_p^n\right)\right]$$

4. The numerical fluxed are computed

$$L_{\overline{p}}^{c,n}\Pi_{\overline{p}}^{c,n}\boldsymbol{N}_{\overline{p}}^{c,n} = L_{\overline{p}}^{c,n}P_c\left(\mathbf{X}_p^n\right)\boldsymbol{N}_{\overline{p}}^{c,n} - \alpha_{\overline{p}}^{c,n}\Delta\boldsymbol{u}_{\overline{a}}^n,$$

$$L_{\underline{p}}^{c,n}\Pi_{\underline{p}}^{c,n}\boldsymbol{N}_{\underline{p}}^{c,n} = L_{\underline{p}}^{c,n}P_c\left(\mathbf{X}_p^n\right)\boldsymbol{N}_{\underline{p}}^{c,n} - \alpha_{\underline{p}}^{c,n}\Delta\boldsymbol{u}_{\underline{a}}^n,$$

where $\Delta\boldsymbol{u}_{\overline{a}}^n$ and $\Delta\boldsymbol{u}_{\underline{a}}^n$ are defined as

$$\Delta\boldsymbol{u}_{\overline{a}}^n = \left[\lambda\left(\Delta\boldsymbol{u}_{cp}^n \cdot \boldsymbol{N}_{\overline{p}}^{c,n}\right)\boldsymbol{N}_{\overline{p}}^{c,n} + (1-\lambda)\,\Delta\boldsymbol{u}_{cp}^n\right],$$

$$\Delta\boldsymbol{u}_{\underline{a}}^n = \left[\lambda\left(\Delta\boldsymbol{u}_{cp}^n \cdot \boldsymbol{N}_{\underline{p}}^{c,n}\right)\boldsymbol{N}_{\underline{p}}^{c,n} + (1-\lambda)\,\Delta\boldsymbol{u}_{cp}^n\right],$$

Solution algorithm

- Two-stage second-order Runge-Kutta scheme
- The solution algorithm for stage 1 is described as:

5. The trajectory equation and governing equations are updated

$$\mathbf{X}_p^{(1)} = \mathbf{X}_p^n + \Delta t \mathbf{u}_p^n,$$
$$\frac{1}{\rho_c^{(1)}} = \frac{1}{\rho_c^n} + \frac{\Delta t}{m_c} \sum_{p \in \mathcal{P}(c)} \left(L_{\overline{p}}^{c,n} \boldsymbol{N}_{\overline{p}}^{c,n} + L_{\underline{p}}^{c,n} \boldsymbol{N}_{\underline{p}}^{c,n} \right) \cdot \boldsymbol{u}_p^n,$$
$$\boldsymbol{u}_c^{(1)} = \boldsymbol{u}_c^n - \frac{\Delta t}{m_c} \sum_{p \in \mathcal{P}(c)} \left(L_{\overline{p}}^{c,n} \Pi_{\overline{p}}^{c,n} \boldsymbol{N}_{\overline{p}}^{c,n} + L_{\underline{p}}^{c,n} \Pi_{\underline{p}}^{c,n} \boldsymbol{N}_{\underline{p}}^{c,n} \right),$$
$$E_c^{(1)} = E_c^n - \frac{\Delta t}{m_c} \sum_{p \in \mathcal{P}(c)} \left(L_{\overline{p}}^{c,n} \Pi_{\overline{p}}^{c,n} \boldsymbol{N}_{\overline{p}}^{c,n} + L_{\underline{p}}^{c,n} \Pi_{\underline{p}}^{c,n} \boldsymbol{N}_{\underline{p}}^{c,n} \right) \cdot \boldsymbol{u}_p^n.$$

17

Typical cases

- Saltzman problem

□ Initial condition

piston moves from the left to right with unit velocity

$$x = (i-1)\Delta x + (11-j)\Delta y \sin[\Delta x(i-1)\pi], \quad y = (j-1)\Delta y,$$

□ Analytical solution

t=0.9, rho = 10, shock reaches the right boundary

□ Uniform 100×10 Cartesian grid. $\lambda = 0$, 0.25, 0.5, 0.75, 1.

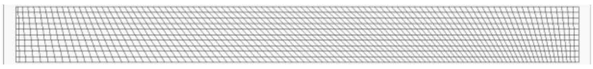

18

Typical cases

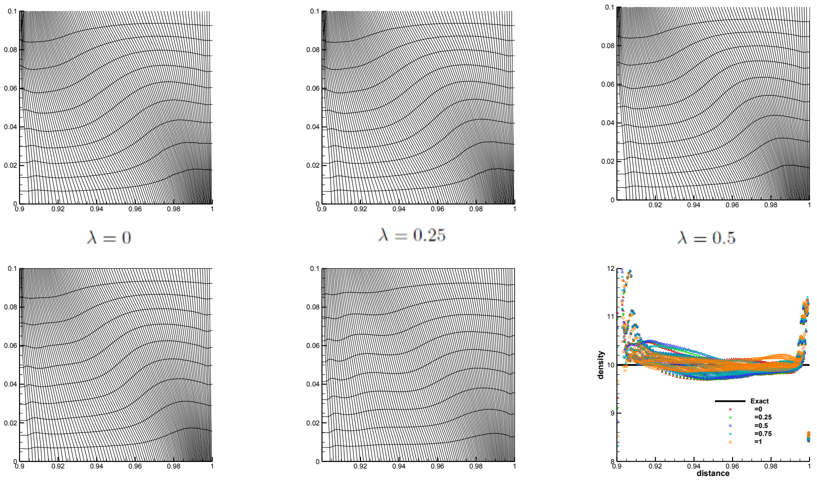

$\lambda = 0$ $\lambda = 0.25$ $\lambda = 0.5$

$\lambda = 0.75$ $\lambda = 1$ density-distance profile

Results of the hybrid nodal solver agrees well with the analytical solution.

Typical cases

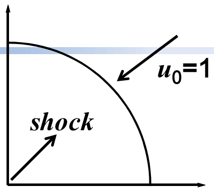

- ◆ Noh problem
  - □ Initial condition

$$[\rho_0,\ \varepsilon_0,\ \mathbf{U}_0(x,y)] = [1, 10^{-6},\ (-x/\sqrt{x^2+y^2},\ -y/\sqrt{x^2+y^2})]$$

  - □ Analytical solution

$$\{\rho, \varepsilon, u_r\} = \begin{cases} \left\{ \left(\dfrac{\gamma+1}{\gamma-1} \right)^d, 0.5, 0 \right\} & \text{if} \quad r < r_s \\ \left\{ \left(1 - \dfrac{t}{r} \right)^d, 0, 1 \right\} & \text{if} \quad r > r_s, \end{cases}$$

  - □ Uniform 50×50 Cartesian grid. $\lambda = 0$, 0.25, 0.5, 0.75, 1.

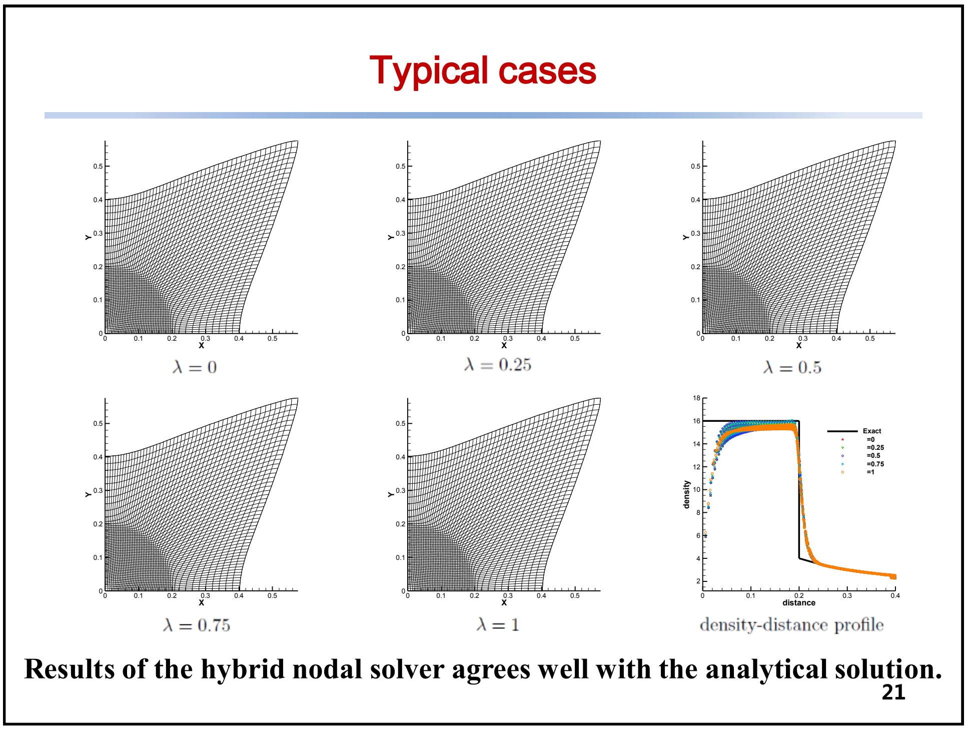

Typical cases

$\lambda = 0$ $\lambda = 0.25$ $\lambda = 0.5$

$\lambda = 0.75$ $\lambda = 1$ density-distance profile

Results of the hybrid nodal solver agrees well with the analytical solution.

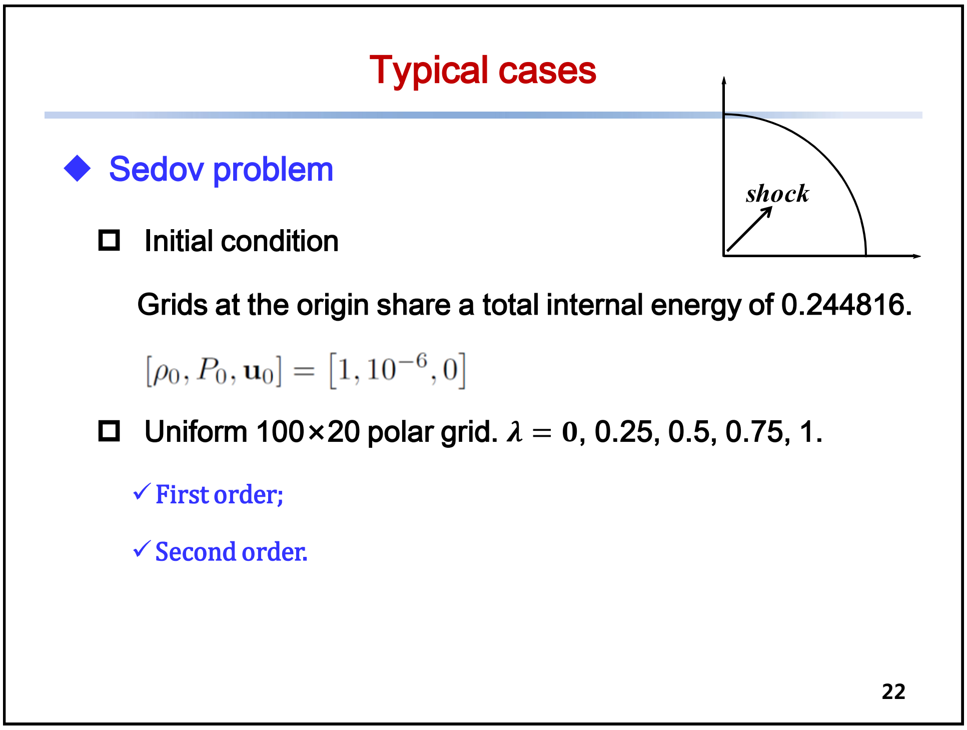

Typical cases

◆ Sedov problem

□ Initial condition

Grids at the origin share a total internal energy of 0.244816.

$$[\rho_0, P_0, \mathbf{u}_0] = [1, 10^{-6}, 0]$$

□ Uniform 100×20 polar grid. $\lambda = 0$, 0.25, 0.5, 0.75, 1.

✓ First order;

✓ Second order.

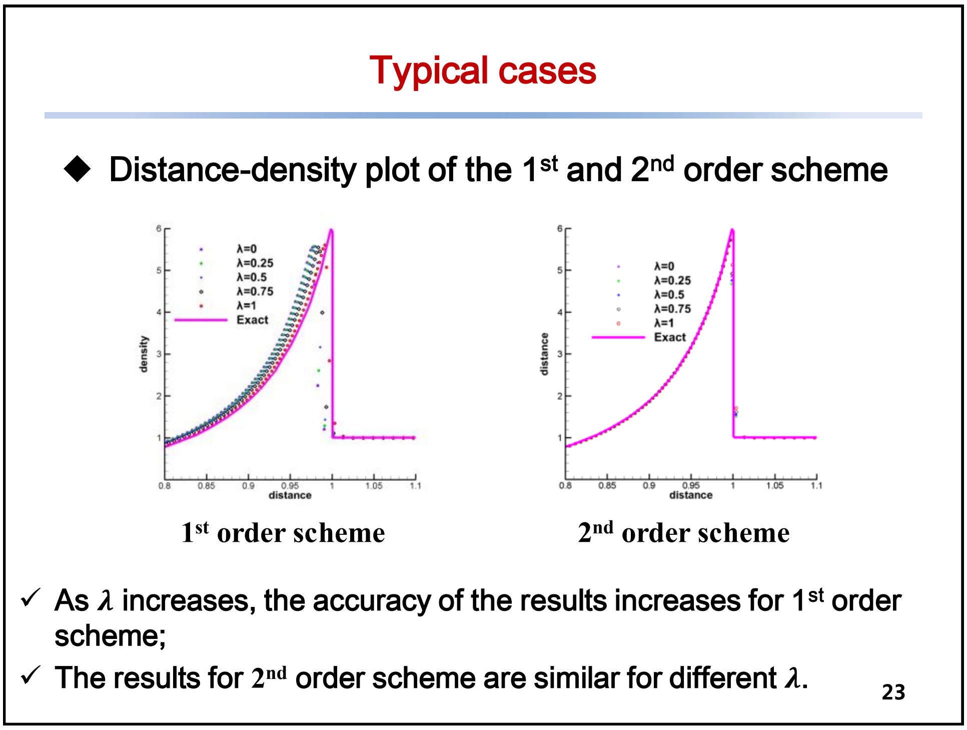

Typical cases

- Distance-density plot of the 1st and 2nd order scheme

1st order scheme

2nd order scheme

- ✓ As λ increases, the accuracy of the results increases for 1st order scheme;
- ✓ The results for 2nd order scheme are similar for different λ.

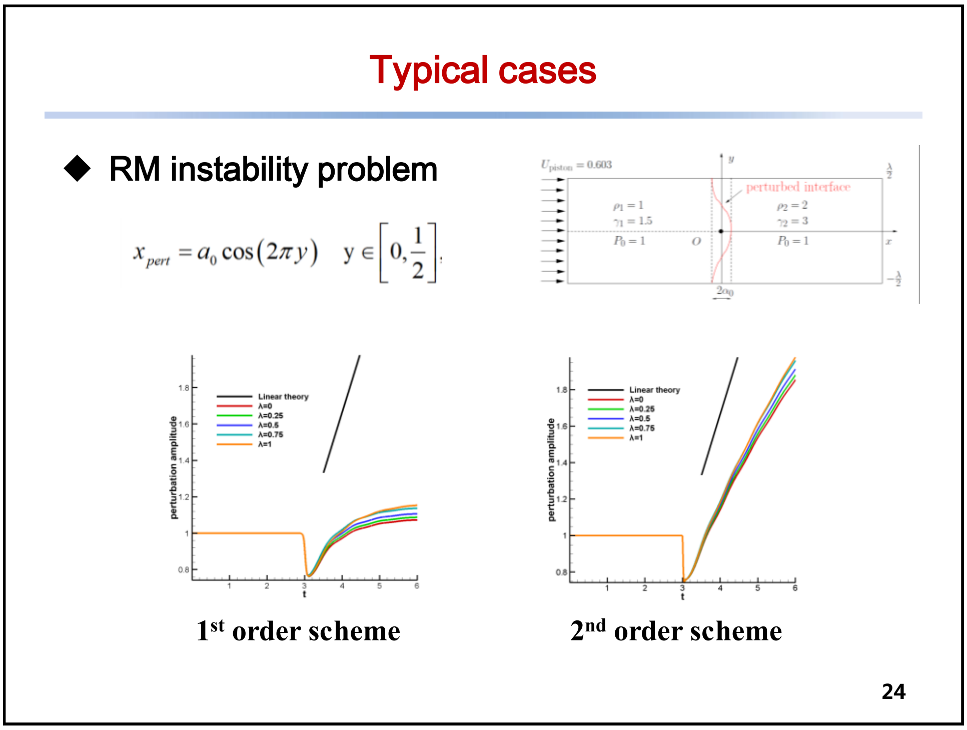

Typical cases

- RM instability problem

$$x_{pert} = a_0 \cos(2\pi y) \quad y \in \left[0, \frac{1}{2}\right],$$

1st order scheme

2nd order scheme

Typical cases

◆ Analysis of the Sedov, Noh and RM instability problem

- ✓ Basically, a larger value of λ means a higher-order approximation of the velocity variable and hence lower diffusivity, it is natural that lower diffusivity provides more accurate results.
- ✓ The differences caused by λ could be reduced in high-order schemes.
- ✓ From the RM instability problem, it is better to set a high value of λ in the 2^{nd} order scheme.

Typical cases

◆ A simplified inertial confinement fusion (ICF) test

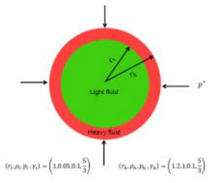
r_l
r_h
Light fluid
Heavy fluid
p^*
$(r_l,\rho_l,p_l,\gamma_l)=\left(1,0.05,0.1,\frac{5}{3}\right)$
$(r_h,\rho_h,p_h,\gamma_h)=\left(1.2,1,0.1,\frac{5}{3}\right)$

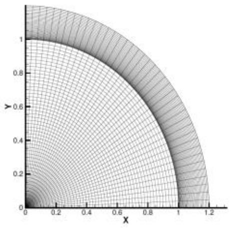

$$p^*(t)=\begin{cases}13 & \text{if} \quad t\in[0,0.04]\\ 13-12.5\times\dfrac{t-0.04}{0.125-0.04} & \text{if} \quad t\in[0.04,0.125]\\ 0.5 & \text{if} \quad t\in[0.125,0.3]\,.\end{cases}$$

- □ Pressure imposed on the outer boundary;
- □ Perturbation of the interface to cause Rayleigh-Taylor instability.

$$r_i^{\text{pert}}=r_i\left[1+a_0\cos(n\theta)\right]$$

- ✓ $a_0=10^{-3}$, $n=8$

Typical cases

□ Material interface at t = 0.3

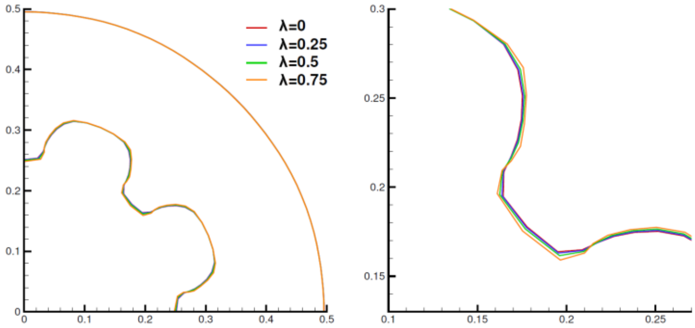

- ✓ The outer interfaces are similar, the inner interfaces are somewhat different.
- ✓ Smaller λ produces smoother material interface because higher dissipation are introduced.

Typical cases

□ Vorticity field at t = 0.3

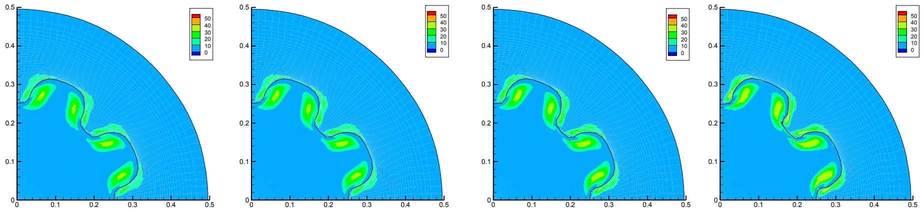

$\lambda = 0$ $\lambda = 0.25$ $\lambda = 0.5$ $\lambda = 0.75$

High vorticity is observed near the interface, this may be physical where the shear effect exists.

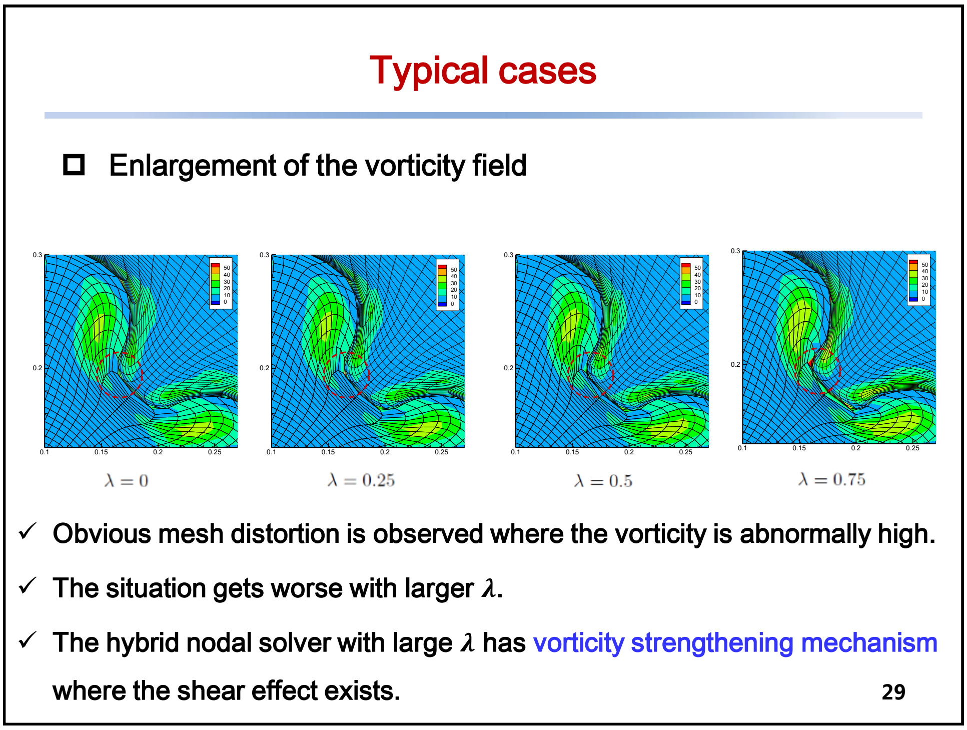

Typical cases

□ Enlargement of the vorticity field

$\lambda = 0$ $\lambda = 0.25$ $\lambda = 0.5$ $\lambda = 0.75$

- ✓ Obvious mesh distortion is observed where the vorticity is abnormally high.
- ✓ The situation gets worse with larger λ.
- ✓ The hybrid nodal solver with large λ has vorticity strengthening mechanism where the shear effect exists.

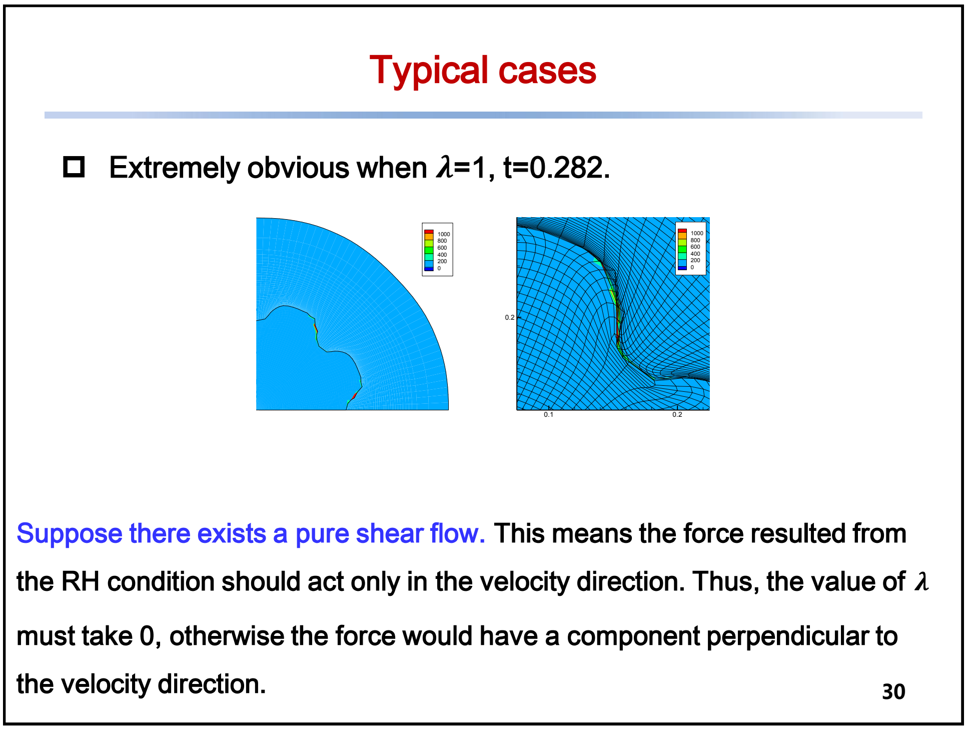

Typical cases

□ Extremely obvious when λ=1, t=0.282.

Suppose there exists a pure shear flow. This means the force resulted from the RH condition should act only in the velocity direction. Thus, the value of λ must take 0, otherwise the force would have a component perpendicular to the velocity direction.

Typical cases

- Selection of λ
  - □ The RT instability problem implies that a higher value of tend to has a vorticity strengthening mechanism.
  - □ Vorticity filtering coefficient

$$\lambda = e^{-|\omega|/5}$$

where ω is defined as the z vorticity. Its value is computed as

$$|\omega| = \left|\frac{\partial v}{\partial x} - \frac{\partial u}{\partial y}\right|$$

Vorticity filtering hybridization

- Sedov problem with 100×20 polar grid
  - □ Distance-density plot of the 1st and 2nd order scheme

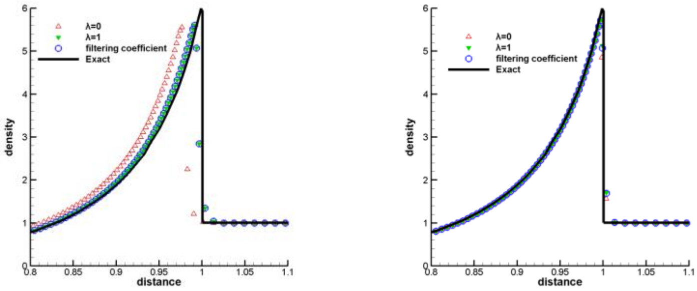

1st order scheme

2nd order scheme

The simulation using vorticity filtering method has high accuracy in both 1st and 2nd order scheme.

Vorticity filtering hybridization

- RM instability problem

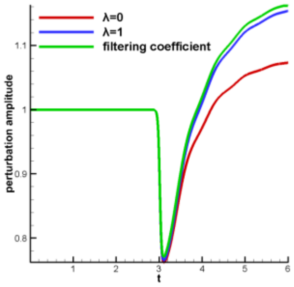

1st order scheme

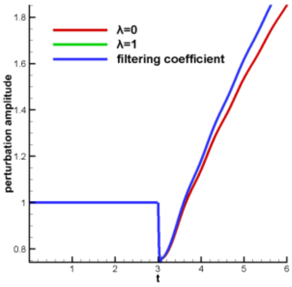

2nd order scheme

The simulation using vorticity filtering method has high accuracy in both 1st and 2nd order scheme.

Vorticity filtering hybridization

- Sedov problem with 50×50 Cartesian grid
  - □ Density profile and final grid of the 1st and 2nd order scheme

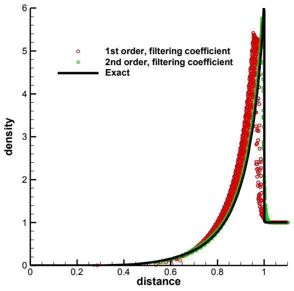

Density profile

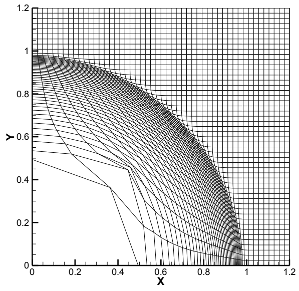

1st order scheme, final grid

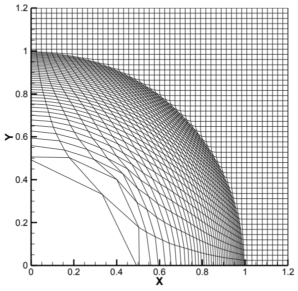

2nd order scheme, final grid

The simulations verify the effectiveness of the vorticity filtering method in Cartesian grid.

Vorticity filtering hybridization

- RT instability problem

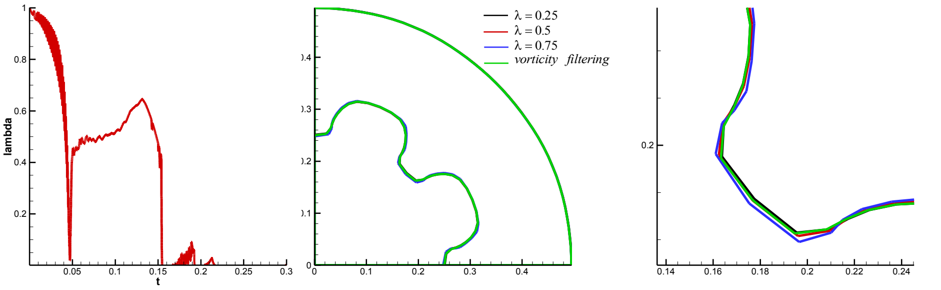

λ vs time matter line enlargement of matter line

The sharpness of the matter line is near the cases when λ is between 0.25 and 0.5.

Conclusion remarks

- □ We propose to use a discrete velocity gradient method to represent the velocity vector in the RH condition.
- □ A hybrid nodal solver with rotation property is thus constructed.
- □ A vorticity filtering method is presented to determine the hybridization strategy.
- □ Numerical cases are presented to prove the effectiveness of the hybrid nodal solver.

THANK YOU

FOR LISTENING!

Appendix A

- Discrete velocity gradient method

$$G_{qc} = G\boldsymbol{N} = \Delta \boldsymbol{u}_{qc}/L_{qc},$$

$$G_{pq} = G\boldsymbol{\tau} = \Delta \boldsymbol{u}_{pq}/L_{pq},$$

$$G\begin{pmatrix} \sin\theta & \cos\theta \\ \cos\theta & -\sin\theta \end{pmatrix} = \begin{pmatrix} \Delta u_{qc}/L_{qc} & \Delta u_{pq}/L_{pq} \\ \Delta v_{qc}/L_{qc} & \Delta v_{pq}/L_{pq} \end{pmatrix},$$

$$G = \begin{pmatrix} \Delta u_{qc}/L_{qc} & \Delta u_{pq}/L_{pq} \\ \Delta v_{qc}/L_{qc} & \Delta v_{pq}/L_{pq} \end{pmatrix} \begin{pmatrix} \sin\theta & \cos\theta \\ \cos\theta & -\sin\theta \end{pmatrix}$$
$$= \frac{\Delta \boldsymbol{u}_{qc} \otimes \boldsymbol{N}}{L_{qc}} + \frac{\Delta \boldsymbol{u}_{pq} \otimes \boldsymbol{\tau}}{L_{pq}}$$

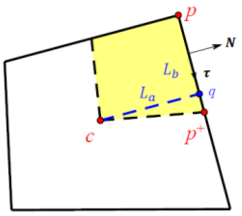

Back

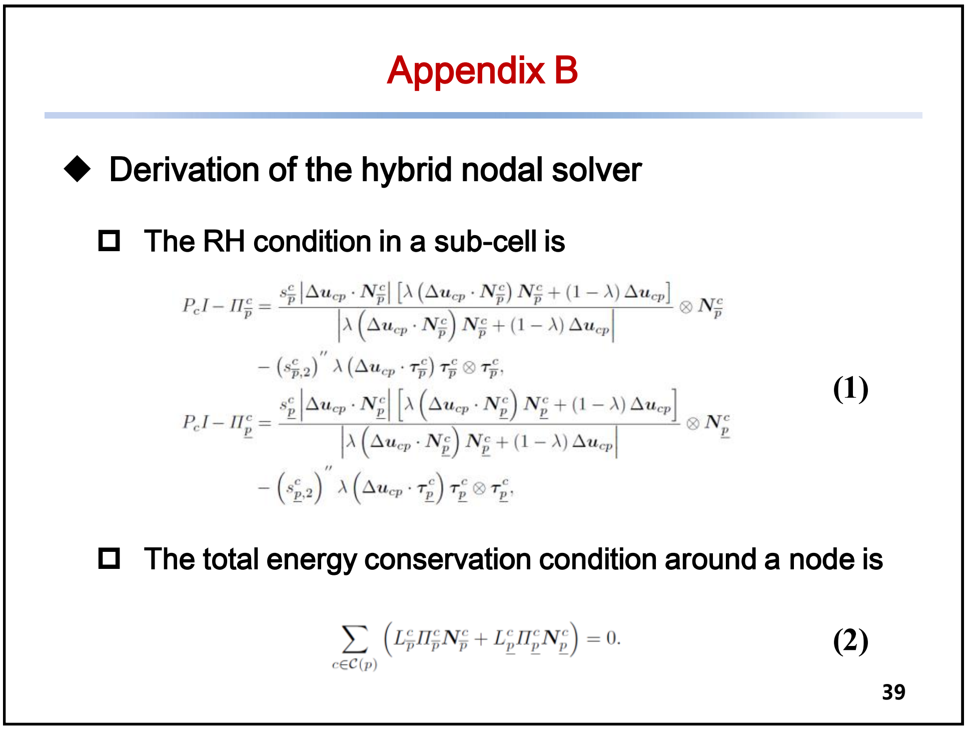

Appendix B

◆ Derivation of the hybrid nodal solver

□ The RH condition in a sub-cell is

$$P_cI-\Pi_{\overline{p}}^c=\frac{s_{\overline{p}}^c\left|\Delta\boldsymbol{u}_{cp}\cdot\boldsymbol{N}_{\overline{p}}^c\right|\left[\lambda\left(\Delta\boldsymbol{u}_{cp}\cdot\boldsymbol{N}_{\overline{p}}^c\right)\boldsymbol{N}_{\overline{p}}^c+(1-\lambda)\Delta\boldsymbol{u}_{cp}\right]}{\left|\lambda\left(\Delta\boldsymbol{u}_{cp}\cdot\boldsymbol{N}_{\overline{p}}^c\right)\boldsymbol{N}_{\overline{p}}^c+(1-\lambda)\Delta\boldsymbol{u}_{cp}\right|}\otimes\boldsymbol{N}_{\overline{p}}^c$$
$$-\left(s_{\overline{p},2}^c\right)''\lambda\left(\Delta\boldsymbol{u}_{cp}\cdot\boldsymbol{\tau}_{\overline{p}}^c\right)\boldsymbol{\tau}_{\overline{p}}^c\otimes\boldsymbol{\tau}_{\overline{p}}^c,$$
$$P_cI-\Pi_{\underline{p}}^c=\frac{s_{\underline{p}}^c\left|\Delta\boldsymbol{u}_{cp}\cdot\boldsymbol{N}_{\underline{p}}^c\right|\left[\lambda\left(\Delta\boldsymbol{u}_{cp}\cdot\boldsymbol{N}_{\underline{p}}^c\right)\boldsymbol{N}_{\underline{p}}^c+(1-\lambda)\Delta\boldsymbol{u}_{cp}\right]}{\left|\lambda\left(\Delta\boldsymbol{u}_{cp}\cdot\boldsymbol{N}_{\underline{p}}^c\right)\boldsymbol{N}_{\underline{p}}^c+(1-\lambda)\Delta\boldsymbol{u}_{cp}\right|}\otimes\boldsymbol{N}_{\underline{p}}^c$$
$$-\left(s_{\underline{p},2}^c\right)''\lambda\left(\Delta\boldsymbol{u}_{cp}\cdot\boldsymbol{\tau}_{\underline{p}}^c\right)\boldsymbol{\tau}_{\underline{p}}^c\otimes\boldsymbol{\tau}_{\underline{p}}^c, \qquad \textbf{(1)}$$

□ The total energy conservation condition around a node is

$$\sum_{c\in\mathcal{C}(p)}\left(L_{\overline{p}}^c\Pi_{\overline{p}}^c\boldsymbol{N}_{\overline{p}}^c+L_{\underline{p}}^c\Pi_{\underline{p}}^c\boldsymbol{N}_{\underline{p}}^c\right)=0. \qquad \textbf{(2)}$$

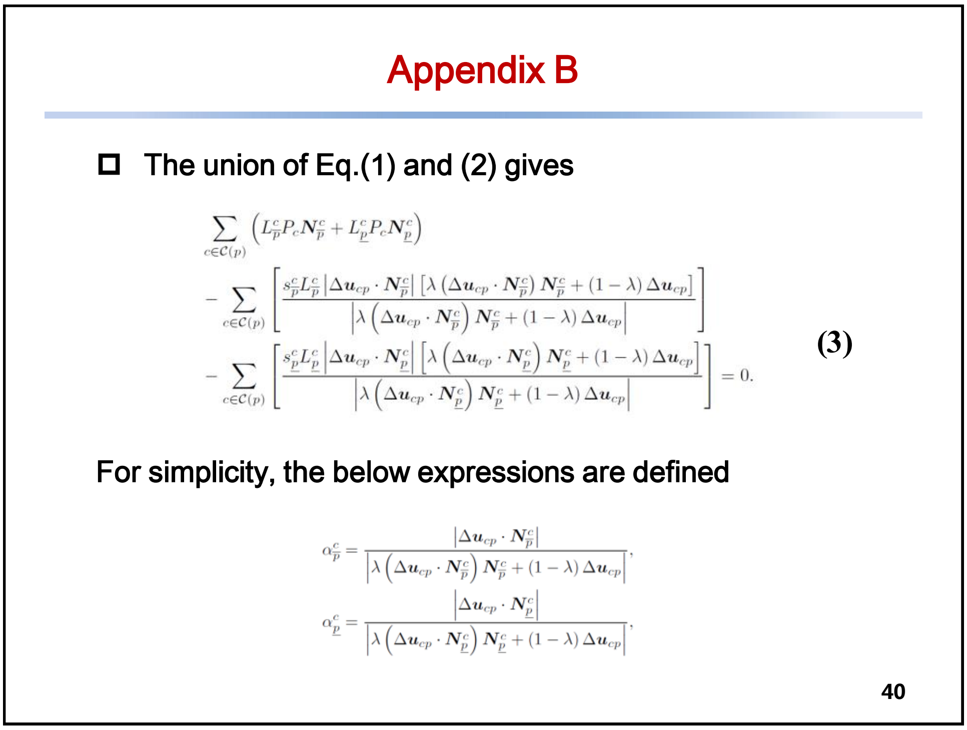

Appendix B

□ The union of Eq.(1) and (2) gives

$$\sum_{c\in\mathcal{C}(p)}\left(L_{\overline{p}}^cP_c\boldsymbol{N}_{\overline{p}}^c+L_{\underline{p}}^cP_c\boldsymbol{N}_{\underline{p}}^c\right)$$
$$-\sum_{c\in\mathcal{C}(p)}\left[\frac{s_{\overline{p}}^cL_{\overline{p}}^c\left|\Delta\boldsymbol{u}_{cp}\cdot\boldsymbol{N}_{\overline{p}}^c\right|\left[\lambda\left(\Delta\boldsymbol{u}_{cp}\cdot\boldsymbol{N}_{\overline{p}}^c\right)\boldsymbol{N}_{\overline{p}}^c+(1-\lambda)\Delta\boldsymbol{u}_{cp}\right]}{\left|\lambda\left(\Delta\boldsymbol{u}_{cp}\cdot\boldsymbol{N}_{\overline{p}}^c\right)\boldsymbol{N}_{\overline{p}}^c+(1-\lambda)\Delta\boldsymbol{u}_{cp}\right|}\right]$$
$$-\sum_{c\in\mathcal{C}(p)}\left[\frac{s_{\underline{p}}^cL_{\underline{p}}^c\left|\Delta\boldsymbol{u}_{cp}\cdot\boldsymbol{N}_{\underline{p}}^c\right|\left[\lambda\left(\Delta\boldsymbol{u}_{cp}\cdot\boldsymbol{N}_{\underline{p}}^c\right)\boldsymbol{N}_{\underline{p}}^c+(1-\lambda)\Delta\boldsymbol{u}_{cp}\right]}{\left|\lambda\left(\Delta\boldsymbol{u}_{cp}\cdot\boldsymbol{N}_{\underline{p}}^c\right)\boldsymbol{N}_{\underline{p}}^c+(1-\lambda)\Delta\boldsymbol{u}_{cp}\right|}\right]=0. \qquad \textbf{(3)}$$

For simplicity, the below expressions are defined

$$\alpha_{\overline{p}}^c=\frac{\left|\Delta\boldsymbol{u}_{cp}\cdot\boldsymbol{N}_{\overline{p}}^c\right|}{\left|\lambda\left(\Delta\boldsymbol{u}_{cp}\cdot\boldsymbol{N}_{\overline{p}}^c\right)\boldsymbol{N}_{\overline{p}}^c+(1-\lambda)\Delta\boldsymbol{u}_{cp}\right|},$$
$$\alpha_{\underline{p}}^c=\frac{\left|\Delta\boldsymbol{u}_{cp}\cdot\boldsymbol{N}_{\underline{p}}^c\right|}{\left|\lambda\left(\Delta\boldsymbol{u}_{cp}\cdot\boldsymbol{N}_{\underline{p}}^c\right)\boldsymbol{N}_{\underline{p}}^c+(1-\lambda)\Delta\boldsymbol{u}_{cp}\right|},$$

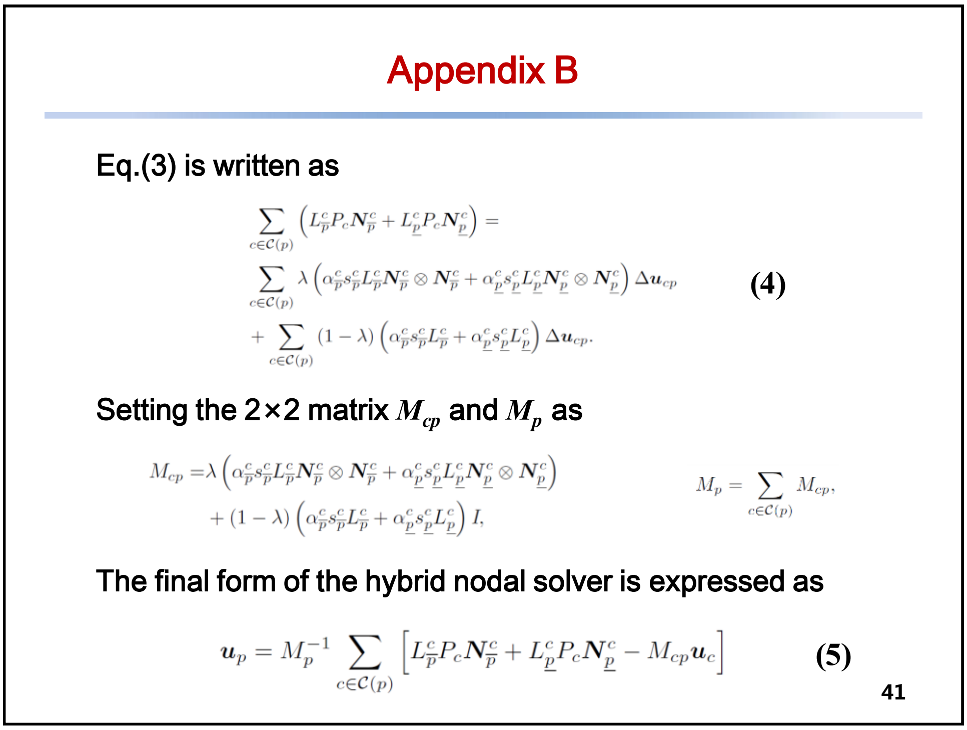

Appendix B

Eq.(3) is written as

$$\begin{aligned}&\sum_{c\in\mathcal{C}(p)}\left(L^c_{\overline{p}}P_c\boldsymbol{N}^c_{\overline{p}}+L^c_{\underline{p}}P_c\boldsymbol{N}^c_{\underline{p}}\right)=\\&\sum_{c\in\mathcal{C}(p)}\lambda\left(\alpha^c_{\overline{p}}s^c_{\overline{p}}L^c_{\overline{p}}\boldsymbol{N}^c_{\overline{p}}\otimes\boldsymbol{N}^c_{\overline{p}}+\alpha^c_{\underline{p}}s^c_{\underline{p}}L^c_{\underline{p}}\boldsymbol{N}^c_{\underline{p}}\otimes\boldsymbol{N}^c_{\underline{p}}\right)\Delta\boldsymbol{u}_{cp}\\&+\sum_{c\in\mathcal{C}(p)}(1-\lambda)\left(\alpha^c_{\overline{p}}s^c_{\overline{p}}L^c_{\overline{p}}+\alpha^c_{\underline{p}}s^c_{\underline{p}}L^c_{\underline{p}}\right)\Delta\boldsymbol{u}_{cp}.\end{aligned}\qquad\textbf{(4)}$$

Setting the 2×2 matrix M_{cp} and M_p as

$$\begin{aligned}M_{cp}=&\lambda\left(\alpha^c_{\overline{p}}s^c_{\overline{p}}L^c_{\overline{p}}\boldsymbol{N}^c_{\overline{p}}\otimes\boldsymbol{N}^c_{\overline{p}}+\alpha^c_{\underline{p}}s^c_{\underline{p}}L^c_{\underline{p}}\boldsymbol{N}^c_{\underline{p}}\otimes\boldsymbol{N}^c_{\underline{p}}\right)\\&+(1-\lambda)\left(\alpha^c_{\overline{p}}s^c_{\overline{p}}L^c_{\overline{p}}+\alpha^c_{\underline{p}}s^c_{\underline{p}}L^c_{\underline{p}}\right)I,\end{aligned}\qquad M_p=\sum_{c\in\mathcal{C}(p)}M_{cp},$$

The final form of the hybrid nodal solver is expressed as

$$\boldsymbol{u}_p=M_p^{-1}\sum_{c\in\mathcal{C}(p)}\left[L^c_{\overline{p}}P_c\boldsymbol{N}^c_{\overline{p}}+L^c_{\underline{p}}P_c\boldsymbol{N}^c_{\underline{p}}-M_{cp}\boldsymbol{u}_c\right]\qquad\textbf{(5)}$$

41